Advanced Output Coupling for High Power Gyrotrons

Grant No. DE-SC0006212

Purpose of the Research

Gyrotrons are the highest energy RF sources in the millimeter and submillimeter-wave frequency range. They are a major component of fusion energy research systems used for plasma heating, plasma current drive, and suppression of plasma instabilities. Energy is extracted from a high power electron beam and converted to a whispering gallery RF mode inside the device. A challenge is efficiently extracting this power from inside the gyrotron vacuum and transporting it to the reactor or other device using the power. Current extraction methods result in significant RF losses and restrict operation of the gyrotron to a small subset of available frequencies. The purpose of this research was to develop an advanced coupling system to eliminate these problems.

Phase II Research

The Phase II program developed an internal RF coupler that transforms the whispering gallery RF mode produced in the cavity to an HE_{11} waveguide mode propagating in corrugated waveguide. This power is extracted from the vacuum using a broadband, chemical vapor deposited (CVD) diamond, Brewster angle window capable of transmitting more than 1.5 MW CW of RF power over a broad range of frequencies. This coupling system eliminates the Mirror Optical Units (MOUs) now required to externally couple Gaussian output power into corrugated waveguide, significantly reducing system cost and increasing efficiency. The program simulated the performance using a broad range of advanced computer codes to optimize the design. Both a direct coupler and Brewster angle window were built and tested at low and high power. Test results confirmed the performance of both devices and demonstrated they are capable of achieving the required performance for scientific, defense, industrial, and medical applications.

Potential Applications

The primary applications for high power gyrotrons are related to the development of fusion energy systems. These devices provide RF power for electron cyclotron heating and RF current drive in tokamak plasmas. They are highly effective in suppressing instabilities in fusion plasmas. Consequently, gyrotrons are a key component in tokamaks around the world. More recently, gyrotrons used to provide dynamic nuclear polarization (DNP) in nuclear magnetic resonance (NMR) spectroscopy. DNP dramatically increases the sensitivity and resolution of NMR spectroscopy for medical imaging and materials research.

Final Technical Report

Advanced Output Coupling for High Power Gyrotrons

Grant Number: DE-SC0006212

Calabazas Creek Research, Inc.
690 Port Drive
San Mateo, CA 94404
(650) 312-9575, Fax: (650) 312-9536
RLI@CalCreek.com

Principal Investigator: Dr. Michael E. Read

Topic Number: 69
Subtopic Number: b

August 2016

Contents

Introduction

Frequency tunable MW gyrotrons are of interest for electron cyclotron resonance heating (ECH), current drive, and suppression of plasma instabilities in tokamak plasmas. Power deposition in the plasma is primarily determined by the magnetic field, so the electron cyclotron resonance interaction between the plasma electrons and the RF wave takes place only in a small region of plasma where the resonance condition is met. While the region being heated can be adjusted by using the Doppler shift with mechanically steerable mirrors in the plasma chamber, the implementation of mechanically steerable mirrors is a challenging and expensive solution. The availability of efficient, frequency tunable, MW gyrotrons would allow simple, fixed, non-steerable mirror antenna systems [2]. Multi-frequency gyrotrons could also suppress neoclassical tearing modes, which require drive current on the high field side without changes in the plasma magnetic field [3]. Consequently, a step tunable gyrotron is being developed by GYCOM and the Institute of Applied Physics for the ASDEX Upgrade ECH system [1].

Gyrotrons are finding increased applications in medical research and treatment. Dynamic Nuclear Polarization (DNP) in Nuclear Magnetic Resonance (NMR) spectroscopy dramatically increases signal levels, enhancing resolution and measurement capabilities. Several organizations are exploring direct couplers for RF power extraction from the gyrotron [4,5].

Modern, MW-level gyrotrons convert the high order (whispering gallery) mode power produced in the circuit to a Gaussian mode using a converter immediately following the cavity. This mode is radiated from a Dimpled-Wall Launcher consisting of a spiral cut in the waveguide (Figure 1). The RF beam is guided and shaped with toroidal mirrors. A final set of approximately planar mirrors with numerically synthesized surfaces (M3 and M4 in Figure 1) reshape the beam to increase the Gaussian content and guide it out the vacuum window. An external Mirror Optical Unit (MOU) converts the Gaussian beam to an HE_{11} mode in corrugated waveguide for transmission to the tokamak. The total RF conversion efficiency, therefore, includes the efficiency of the launcher, focusing mirrors, and MOU. Figure 2 shows a photograph of a 110 GHz gyrotron and MOU connected the DIII-D transmission line at General Atomics. The direct coupler developed in this program eliminates the MOU with the HE_{11} transmission line connected directly to an output flange on the gyrotron. Each MOU costs approximately $500,000 per gyrotron, including the cost of fabrication, installation, and lost RF power [6].

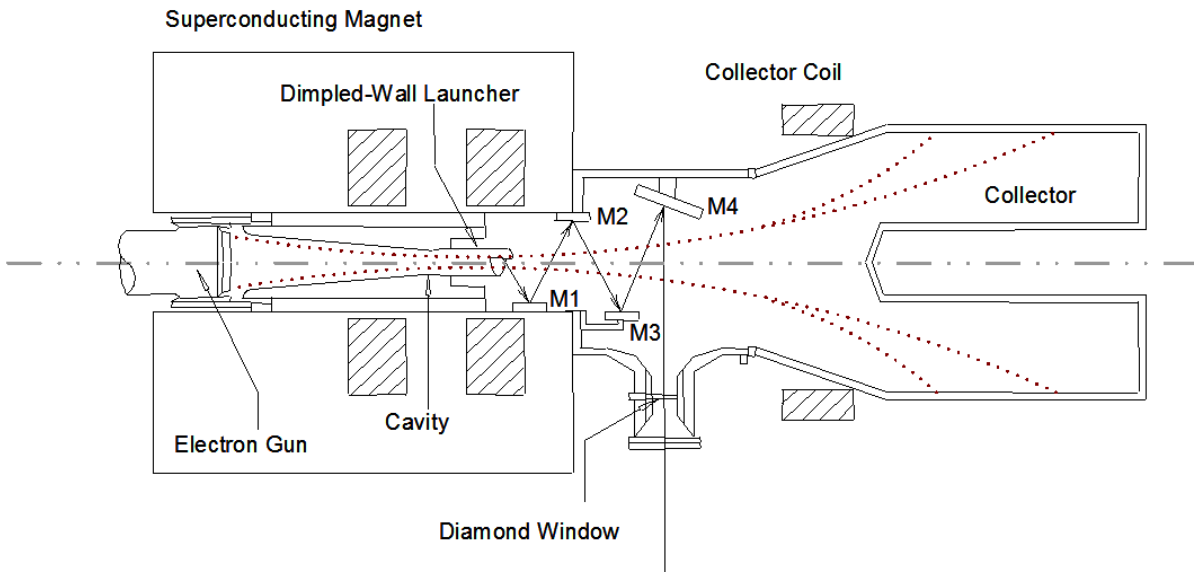

Figure 1. Schematic of gyrotron with Gaussian RF output

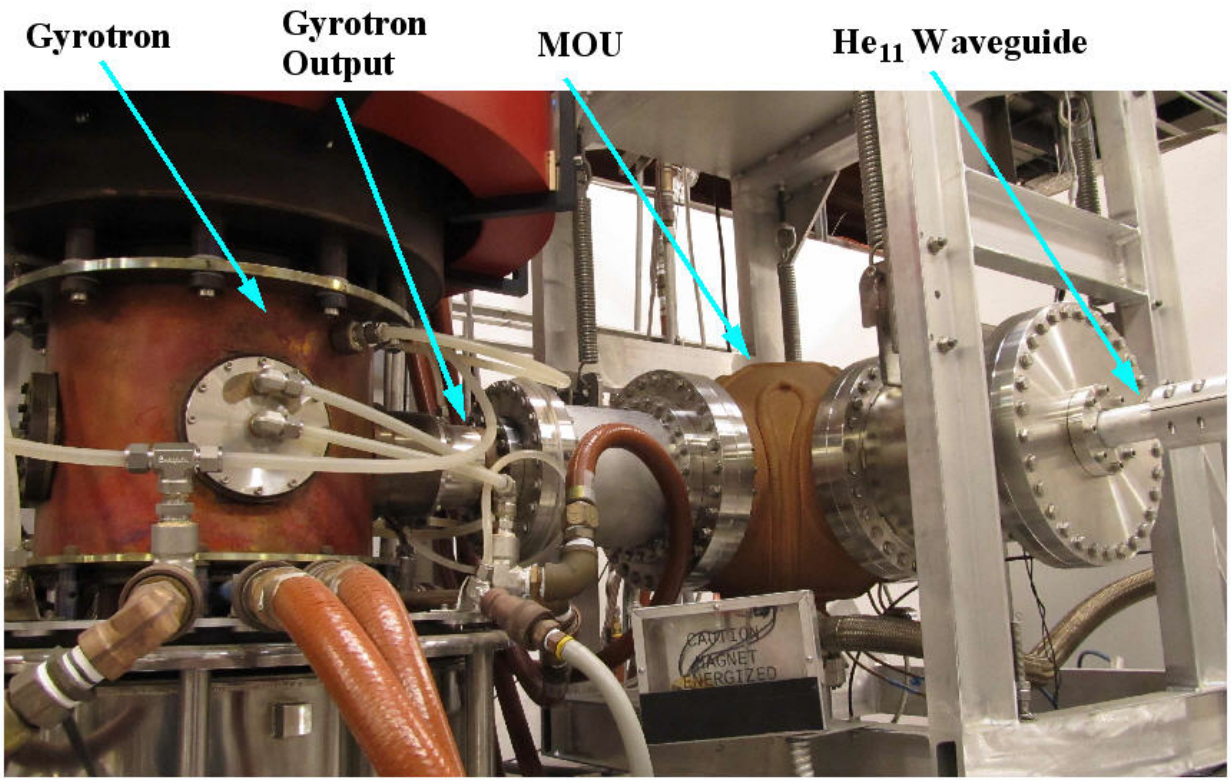

Figure 2. Photograph of 110 GHz gyrotron with Mirror Optical Unit connected to HE11 transmission line

Multi-frequency gyrotron operation is achieved by changing the magnetic field in the cavity to initiate oscillations in different resonant modes. Experiments demonstrated that multi-frequency gyrotrons can be built with good cavity efficiency at MW power levels. A Russian team, in collaboration with German partners, developed a dual frequency gyrotron for 105-140 GHz operation [7], and developers at the Japanese Atomic Energy Agency (now QST), developed a dual frequency gyrotron that produced 1.4 MW at 110 GHz and 1.2 MW at 138 GHz [8]. QST also built and tested a gyrotron producing RF power at 203, 170, 137, and 104 GHz [9].

Before the RF power can be used, however, it must be extracted from the gyrotron vacuum and coupled into HE_{11} waveguide. The multi-frequency gyrotrons mentioned above produced RF power where the thickness of the window represented multiples of a half wavelength of the RF frequency. This limits operation to a set of discreet frequencies. Putting the window at the Brewster angle allows transmission at essentially all frequencies. German developers recently reported a multi-frequency, megawatt gyrotron incorporating a Brewster angle window [10]. The Brewster window allowed operation of the German gyrotron at ten frequencies between 111.6 and 165.7 GHz.

Currently, chemical vapor deposited (CVD) diamond is the only material with sufficiently low loss and high strength capable of transmitting long pulse, mm-wave power at megawatt levels. Incorporating a diamond window into a gyrotron is quite difficult, even with a circular window. The geometry required for a Brewster window makes the problem even more difficult. The challenge is addressing the mechanical stresses associated with brazing CVD diamond into a metal support structure comprising part of the gyrotron vacuum envelope.

Following the output window, the challenge for multi-frequency gyrotrons is efficiently converting the RF power from the cavity into an HE_{11} mode propagating in corrugated waveguide. The problem begins at the quasi-optical launcher, where each frequency is launched with slightly different radiation characteristics due to differences in the bounce angle in the output waveguide. In general, the geometry of the launcher can be optimized for one frequency; however, this problem can be minimized by an improved optimization technique recently developed by Sobolev and Denisov based on the reciprocity theorem [11]. The algorithm is neither mode nor geometry specific. In addition, the algorithm converges monotonically, thus requiring significantly fewer iterations than typical optimization techniques.

Any differences in Gaussian mode characteristics generated at the launcher can be magnified by the subsequent mirrors that shape and focus the power through the output window. In practice, the various frequencies contain different percentages of the pure TEM_{00} mode and propagate at slightly different angles. This provides additional challenges for the output window and the MOU. The output window must be sufficiently large to allow extraction of RF power at frequencies not focused to the center of the window. This becomes problematic for expensive CVD diamond windows.

Even for single mode operation, a few percent of the RF power is typically lost in the MOU. JAEA measured the transmission of various frequencies after approximately forty meters of HE_{11} transmission line. The line contained seven bends, which resulted in additional loss, so only the relative percentages of power at each frequency can be compared. The transmission efficiency was 90.7%, 89.6%, and 84.5% for 170 GHz, 137 GHz, and 104 GHz, respectively.

Calabazas Creek Research, Inc. (CCR) is addressing these issues by directly coupling multi-frequency, gyrotron power from the launcher directly into HE_{11} waveguide incorporating a Brewster angle diamond window. This results in the following advantages over existing technology:

- Separate focusing and phase correcting mirrors inside the gyrotron are eliminated, reducing cost and lost RF power,
- The diamond window is smaller, since power at all frequencies is contained and centered in the waveguide,
- The MOU is eliminated, reducing cost and improving efficiency.

Figure 3 compares the launcher, mirror system, and output window for a typical high power gyrotron with the configuration incorporating the direct coupler and Brewster angle window. The Brewster angle window is approximately the same size as the circular window and considerably smaller than the diamond Brewster angle window in the German gyrotron. Never the less, it can transmit more than 1.8 MW CW of RF power.

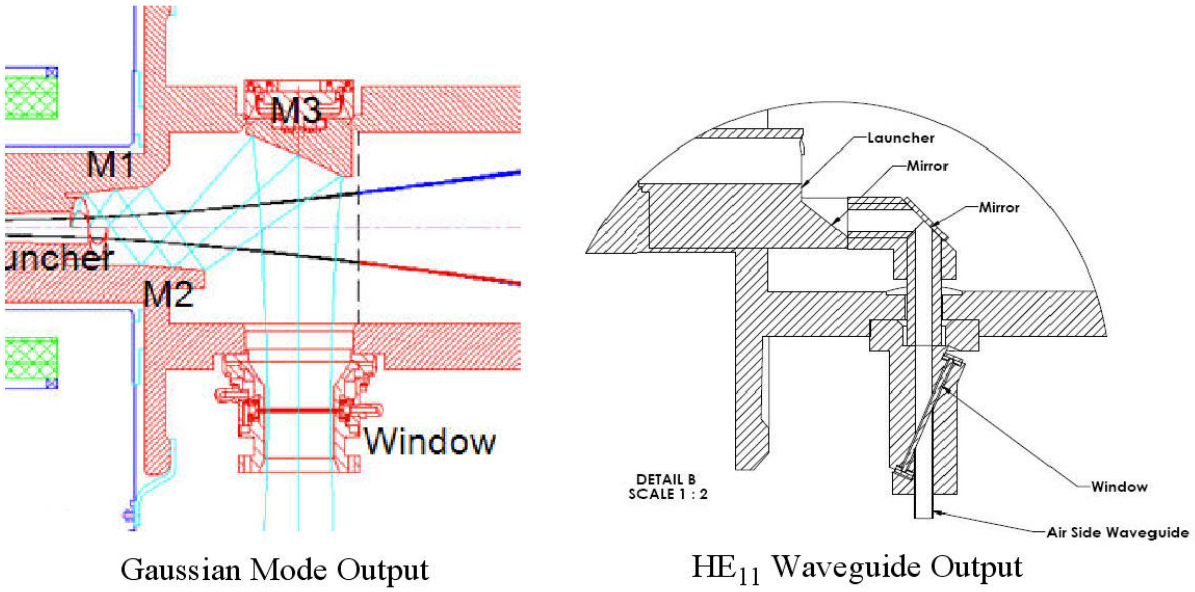

Figure 3. Comparison of existing multi-mirror launcher systems and Gaussian mode output with direct coupler, Brewster window, and waveguide output.

This report describes the design of the direct coupler and Brewster angle window and presents experimental measurements of performance.

Direct Coupler

Design and Fabrication

Simulation of quasioptical launchers requires precise simulation of the RF field propagating through the circular waveguide from the cavity and the fields of the free space wave launched from the spiral cut. This also requires design and simulation of small dimples in the launcher section of the guide to properly shape the RF field for efficient generation of the free space wave. CCR revolutionized the design of these launchers through development of an advanced code that solves surface field integral equations for the RF wave [13,14]. The resultant code, SURF3D, was developed under a previous SBIR program, and this technology is now used worldwide for gyrotron development [15].

CCR's SURF3D code is based on the electric surface integral equation and the computation is accelerated by the multi-level fast multipole technique. The code made high-accuracy analysis of quasioptical (QO) launchers quite tractable with memory requirements of a few GBs of RAM and only tens of minutes of CPU time. With this code the task of designing an internal coupler to focus RF power into corrugated waveguide became feasible on a typical high-end PC.

The approach for internally coupling RF power into corrugated waveguide is based on modification of the existing QO launcher technology. The radiated field from QO launchers, while Gaussian in profile, is highly elliptical, with the azimuthal beam waist size being typically a quarter to a fifth the longitudinal waist size. In addition the azimuthal beam waist size is very narrow (on the order of a few wavelengths), so there is a rapid azimuthal divergence of the beam as it radiates from the launcher. In order to couple efficiently to the HE_{11} mode in a corrugated waveguide it is necessary to modify the radiated field from the launcher to greatly reduce the azimuthal beam divergence and ellipticity. This can be accomplished by modifying the latter part of the launcher design so the Gaussian beam is transformed to a less elliptical shape. Thus the length of the launcher is the same as the original launcher and maintains the same clearance from the electron beam. A single mirror placed on the outer envelope of the

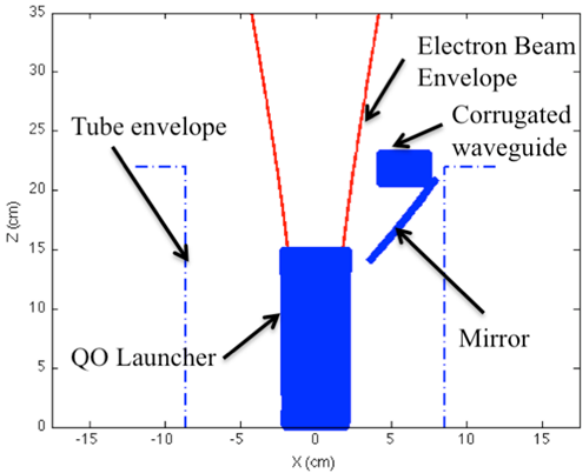

Figure 4. Internal coupler approach

gyrotron matches the beam waist to the HE_{11} mode in the corrugated guide and corrects the output beam angle tilt to be parallel to the tube axis (Figure 4).

CCR designed and built a prototype, direct coupler for low and high power RF testing. The design started with a 110 GHz QO launcher in a gyrotron at the Massachusetts Institute of Technology Plasma Science and Fusion Center (MIT). The beam generated by this launcher exhibits a waist size of 0.25 cm and 1.23 cm in the azimuthal and longitudinal directions, respectively, and radiates from the launcher with an angle of 65 degrees with respect to the tube axis. After modification of the launcher design, the output beam waist diameter was transformed to 0.9 cm and 1.0 cm in the azimuthal and longitudinal directions, respectively.

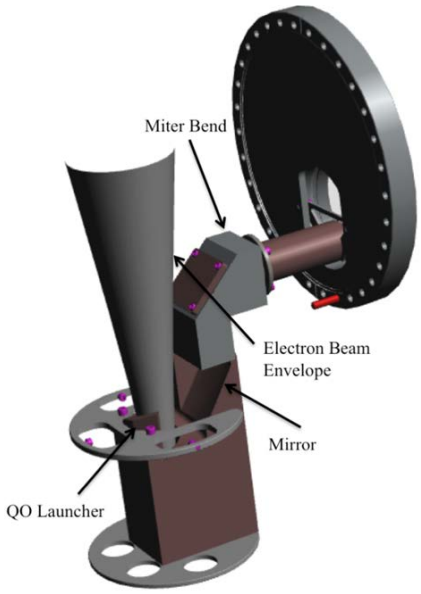

Figure 5. Solid model of internal coupler prototype

The design of the single matching mirror was numerically optimized to provide maximum coupling to the HE_{11} mode in the corrugated waveguide. The simulated coupling efficiency (power in HE_{11} mode / power in cavity mode) for the design is 97.4%. About 1.3% of the incident cavity power is not coupled into the waveguide. The HE_{11} mode purity is 98.8%. In this design, only the latter part of the launcher and matching mirror were optimized. With optimization of the converter section of the QO launcher, it is likely that the coupling efficiency and HE_{11} mode purity could be improved to better than 99%.

The direct coupler was designed for drop-in installation into the MIT gyrotron. A solid model of the coupler mechanical design is shown in Figure 5, and a photograph is shown in Figure 6. Since the mirror is very close to the launcher, machining of the launcher and mirror was performed in a single operation. This insures proper alignment of the launcher and mirror focusing system. In addition to the launcher and mirror, a miter bend directs the output power radially from the gyrotron.

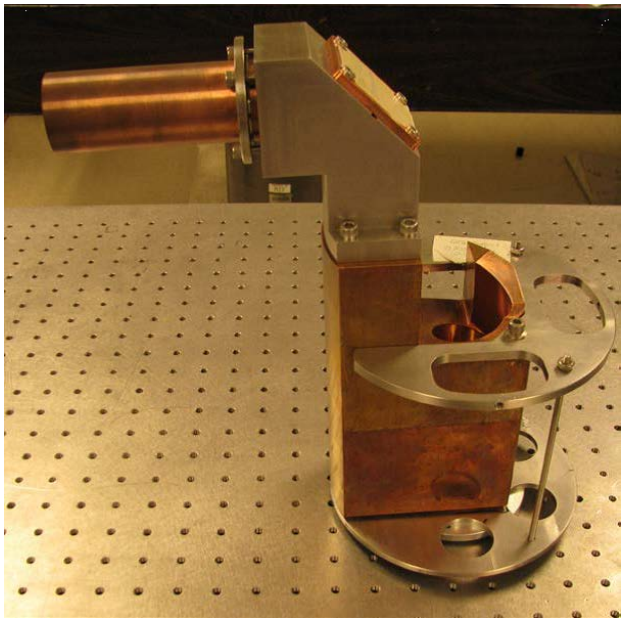

Figure 6. CCR direct coupler

Testing

Cold Testing

Both low and high power tests were performed using facilities at MIT. Low power measurements included scans of the amplitude and phase of the RF power radiated from the direct coupler using the measurement system Figure 7. The coupler was designed to convert the $TE_{22,6}$ mode into the HE_{11} mode in corrugated waveguide. A mode generator produced the $TE_{22,6}$ mode.

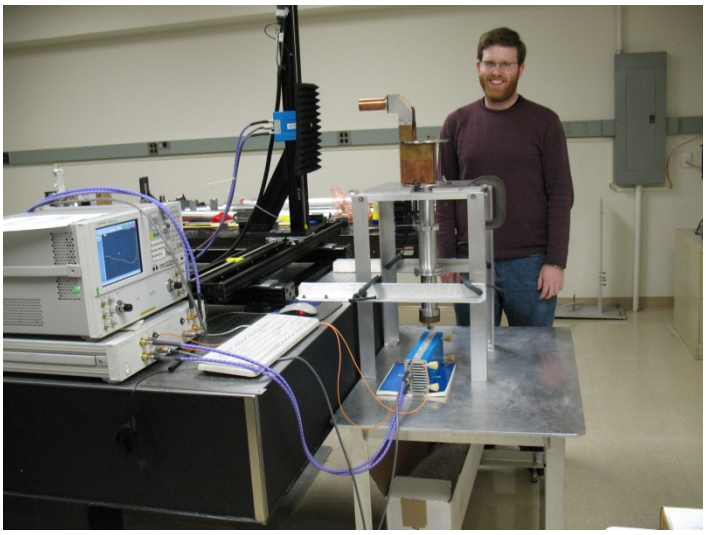

Figure 7. Low power test measurement system for the direct coupler

To maximize accuracy, the radiation pattern was measured on multiple planes normal to the axis of the converter output. Figure 8 shows the antenna pattern 7 cm from the waveguide aperture. MIT used two different methods to determine the mode purity from the antenna scans. The first method uses amplitude and phase data measured independently on each of three planes. The measurements on each plane completely characterize the RF fields, so the measurements from multiple planes verify consistency. MIT also used the phase retrieval method, where data from several planes are combined to define the fields. The agreement from the two methods was very good. The measurements indicated that the HE_{11} content in the converter output waveguide was 97.9 ± 0.25 %, which is higher than that for MIT's four-mirror mode converter [16].

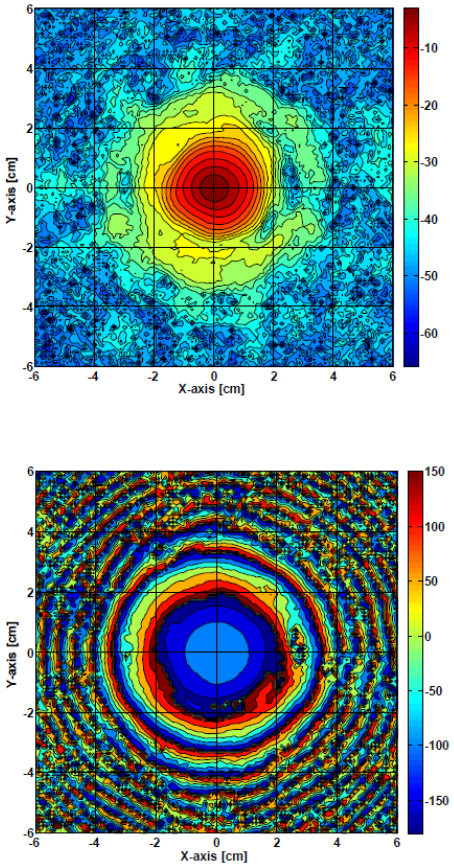

Figure 8. Radiation patterns from the CCR direct coupler

These results significantly exceeded expectations, since the measurements also included the effect of a right angle bend between the coupler and the HE_{11} waveguide output. It was anticipated that the bend would add approximately 2% mode conversion. Transmission of approximately 98% HE_{11} mode from the output waveguide confirmed that the coupler,

right angle bend, and output waveguide are highly efficient in extracting RF power from gyrotrons into transmission lines. Recall that current gyrotrons with MOUs lose approximately 7% of the RF power generated by the cavity.

Testing on a 110 GHz Gyrotron

The coupler was installed in the MIT gyrotron for high power testing. The MIT experimental gyrotron operates at 110 GHz in the $TE_{22,6}$ mode with a magnetic field of 4.4-4.5 T. MIT increased the magnetic field to 7 T to test a 170 GHz gyrotron; however, they currently limit field strengths to less than 5.5 T. The 5.5 T field allows operation to 135 GHz, which is 23% above the 110 GHz frequency. The magnet would, of course, operate at magnetic fields less than 4.0 T.

Following the high power tests, it was determined that the gyrotron was not operating properly. The measured output power was significantly below expectations, and subsequent operation of the gyrotron with a standard quasi-optical coupler and mirror system produced similar results. It was determined that the electron gun was seriously damaged, which significantly impact performance of the RF cavity. This reduced the output power to approximately half that achieved in prior tests. MIT is replacing the gun and will repeat the direct coupler tests as soon as the gyrotron is available. Never the less, some important results were obtained.

A schematic layout of the MIT gyrotron is shown in Figure 9. A superconducting magnet produces the cavity magnetic field (Bo) required for the resonant interaction between the beam electrons and the cavity electromagnetic field; in this case for the $TE_{22,6}$ mode. The fringe field

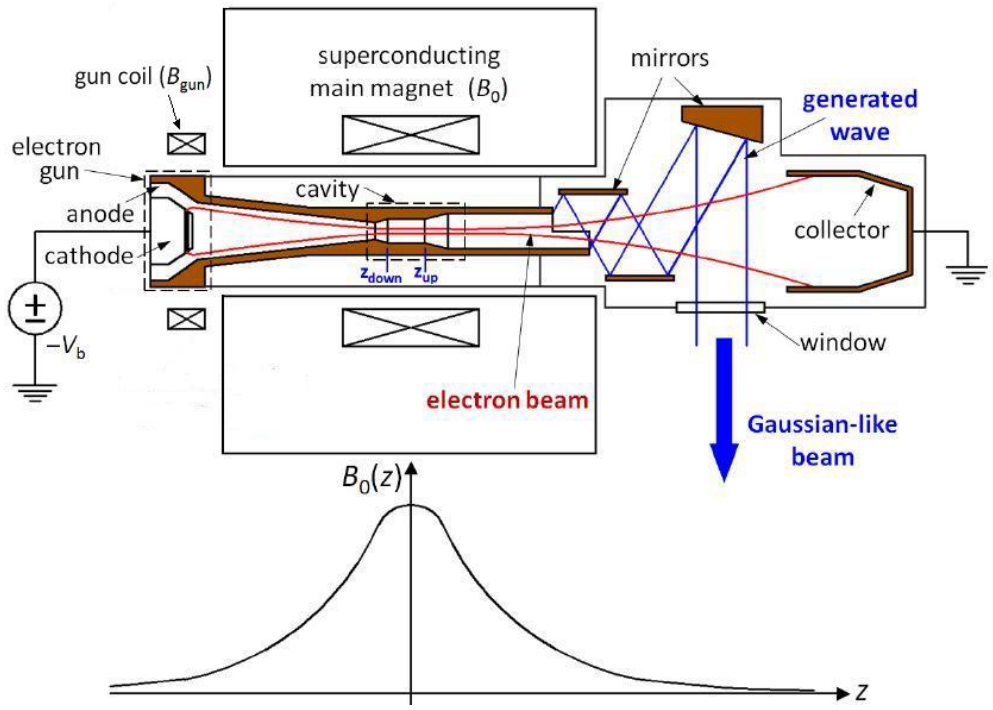

Figure 9. Schematic of 110GHz gyrotron and axial magnetic field profile

of the superconducting magnet plus the local magnetic field from the gun coil determine the cathode magnetic field Bgun and the electron velocity ratio ($\alpha = \upsilon\perp/\upsilon\|$, where $\upsilon\perp$ and $\upsilon\|$ are the electron velocity components relative to the magnetic field). In the standard configuration, microwaves leaving the cavity are launched by the tapered helix-cut mode converter and focused into a Gaussian-like beam by the four-mirror, optical system.

Previous test with MIT's four-mirror output coupler achieved typical high efficiency output power of 1.2 – 1.3 MW, with the most stable operation producing 0.6 – 0.7 MW. Powers obtained with the CCR direct coupler were approximately half these values. CCR performed extensive simulations to understand this performance, however, simulations confirmed that the coupler should provide similar, if not better, performance than the four-mirror coupler. Subsequent test of the four-mirror coupler revealed the damaged condition of the electron gun described earlier.

Measurement of the radiation pattern from the gyrotron successfully reproduced the pattern achieved during low power testing. Figure 10 shows the measured radiation patterns. The measured HE_{11} mode content was 97.5 $\pm$ 1%. This confirmed that the direct coupler was performing as designed, despite the reduced power generated by the RF cavity.

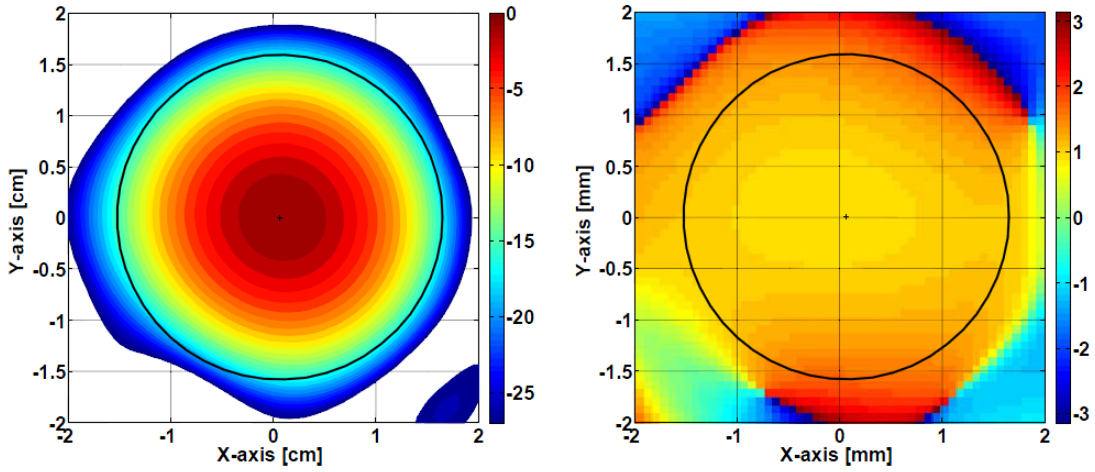

Intensity at corrugated waveguide output. Phase at corrugated waveguide output.

Figure 10. Intensity and phase profiles for CCR mode coupler hot-test

The MIT electron gun was replaced in September 2016, and the gyrotron is being conditioned to full power operation using the four-mirror output coupling system. Tests of the direct coupler are scheduled for early 2017.

Brewster Angle Window

Design and Fabrication

The principal design parameter of a Brewster window is the angle, θ_B, between the normal to the window and the axis of the waveguide. For a free space wave and a window in air, this angle is given by [17]

$$\theta_B = \text{atan}(n_2) \quad (1)$$

where n_2 is the index of refraction for the window material. For diamond used in gyrotron windows, n_2 is 5.7, and the Brewster angle is 67.27°. The power reflection for diamond as a function of angle is given in Figure 11. The reflection remains below 1% (-20 dB) between 61 and 71 degrees.

The Brewster angle is independent of the window thickness. Given the cost of diamond, the window need only be as sufficiently thick to resist atmospheric pressure and survive fabrication stresses. If the window can be supported by an elliptical surface, a Brewster window can be thinner than currently used in 106 mm diameter round windows. The CVD diamond window in this program was 101.6 mm along the major axis and 38.1 mm along the minor axis with a thickness of 1.5 mm. For reference, the CVD diamond window for the Gaussian mode in the German gyrotron was 139 X 95 X 1.7 mm [10].

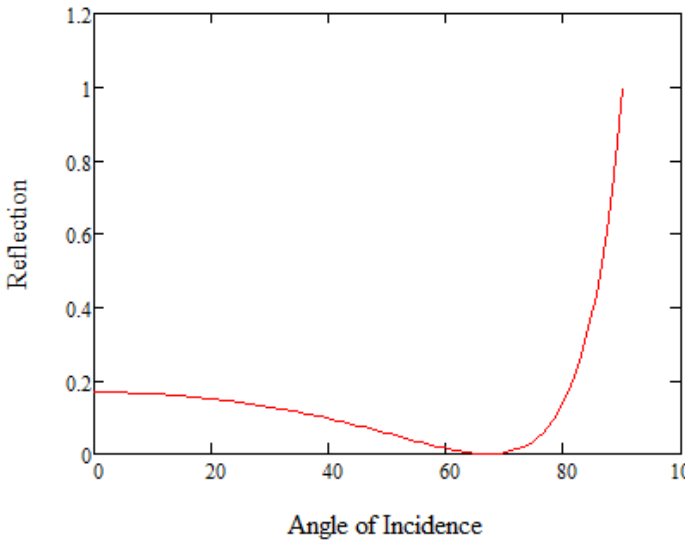

Figure 11. Reflected power of a CVD diamond window as a function of the angle between the normal to the window and the wave axis.

These calculations apply to a linearly polarized plane wave. The CCR window is mounted in 1.25 inch (31.75 mm) diameter corrugated waveguide supporting the HE_{11} mode. The cross polarized components of this mode exhibit a 17 percent reflection; however, these components are negligibly small [18]. At frequencies over 100 GHz, the wave propagation angle in the highly overmoded guide is approximately 1.5°. From Equation (1), it can be seen that this effective spread in angle will present a negligible effect.

Of more concern is the displacement of the wave axis as it goes through the window, shown in Figure 12. The displacement is not important in free space, but results in an asymmetry in waveguide that can result in mode conversion and reflection. It was anticipated in the Phase I program that this could be mitigated by displacing the axis of the output waveguide to "follow" the wave.

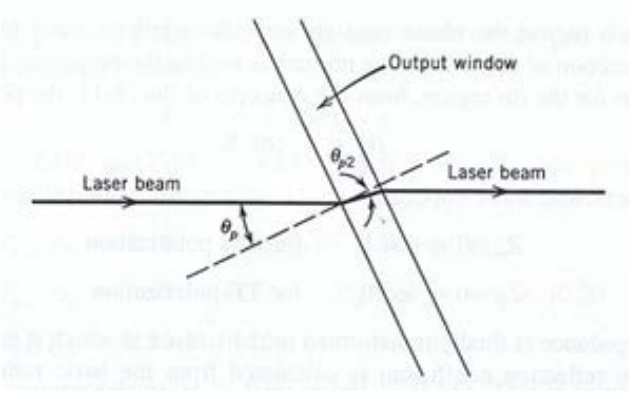

Figure 12. Sketch showing the offset of a wave vector as it goes through a Brewster window [17].

To confirm this hypothesis, CCR performed simulations using ANSYS/ANSOFT's High Frequency Structure Simulator (HFSS) using the model shown in Figure 13. It contains the detailed waveguide structure with the window inserted into the guide. To minimize run time and memory usage, half of the structure was modeled with a "perfect H" boundary at the symmetry plane and perfectly absorbing boundaries at the ends. These are shown as outlines in the figure. A Gaussian source was placed just inside the left hand end of the structure.

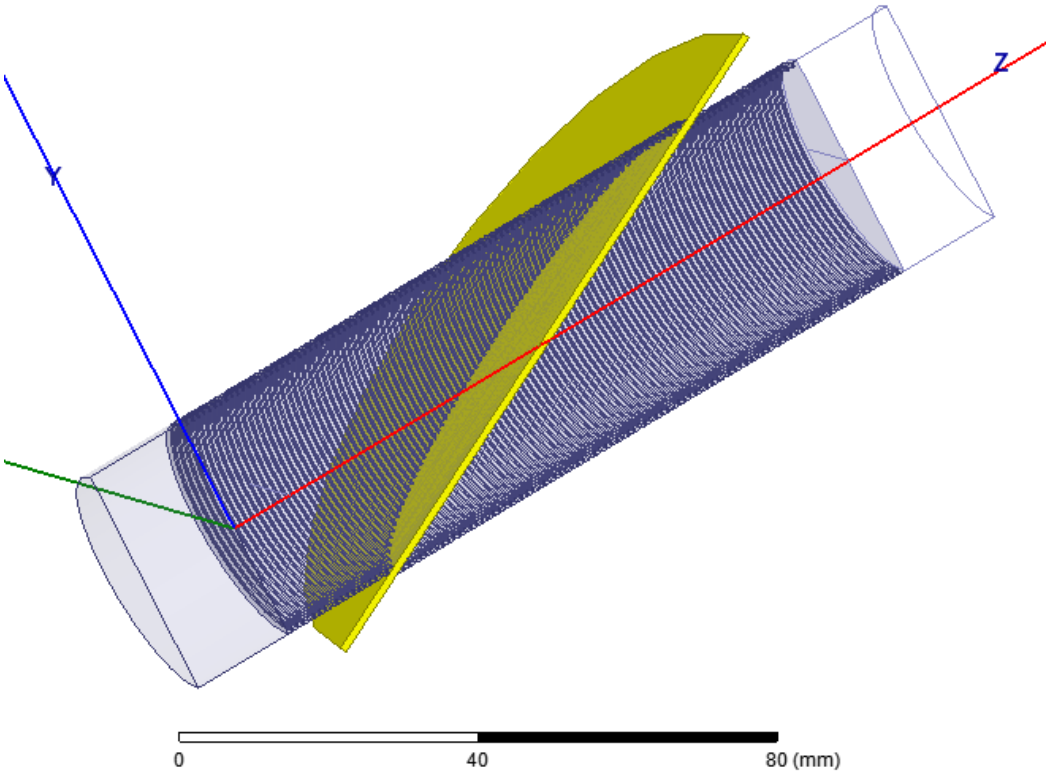

Figure 13. HFSS model of the Brewster window

The waveguide is highly overmoded and involves the very small scale corrugations in the waveguide wall; consequently, simulations required significant computer resources. Ideally, one would include a significant section of waveguide between the source and the window to ensure that modes not supported by the waveguide evanesced by the time they reached the window. Simulation of the geometry in Figure 13 required approximately twenty four hours to execute on a 12 core 3.46 GHz Xeon processor. More importantly, simulations used about 64 GB of the available 72 GB of memory. Therefore, it was anticipated that some mode impurity would be inherent in the model and the results would indicate a lower bound on the mode purity. The simulations were used to guide the experimental window design with low power RF test measurements providing window performance information in Task 3.

Previous experience with single frequency, single disk windows and preliminary thermo-mechanical analysis indicated the minimum window thickness should be 1-1.5 mm. Simulation results for a 1.5 mm window are shown in Figures 14 and 15.

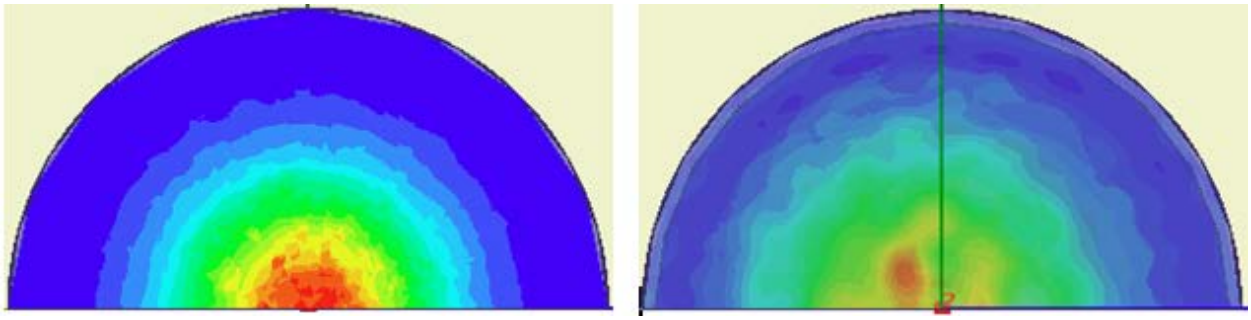

Figure 14. Power contours on cross sections at the input (left) and output (right) of the corrugated waveguide for the 1.5 mm diamond window with the axes of the input and output waveguides coincident. The softening of the colors in the right hand figure is due to the HFSS display.

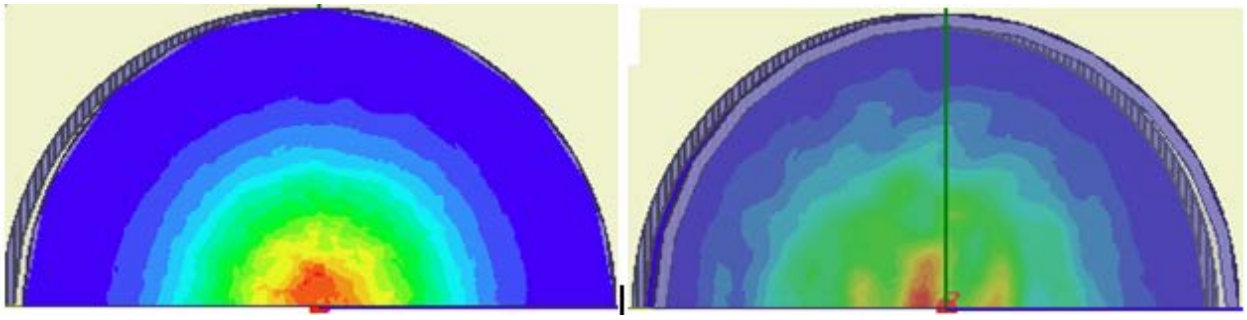

Figure 15. Power contours on cross sections at the input (left) and output (right) of the corrugated waveguide for the 1.5 mm diamond window with the axes of the output waveguide offset to compensate for the wave vector shift. The softening of the colors in the right hand figure is due to the HFSS display.

CCR used information from this task to design the Brewster angle window for thermomechanical analysis in Task 2 and testing in Task 3.

Initial thermal analysis focused on the power transmission capability of the window [19]. Figure 17 shows the peak temperature versus aperture size for a diamond Brewster window transmitting 1.5 MW of continuous power at 170 GHz. This simulation assumed a loss tangent of 4 x 10^{-5}. The window thickness was 1.6 mm, and the disk was tilted 62.5^{o} with respect to the waveguide axis. This result indicates the window disk major axis could be as small as 51 mm, well below the CCR design. In addition, the measured loss tangent in the CCR window was approximately 2 x 10^{-5}, implying that the window should be capable of transmitting more than 2 MW of continuous RF power.

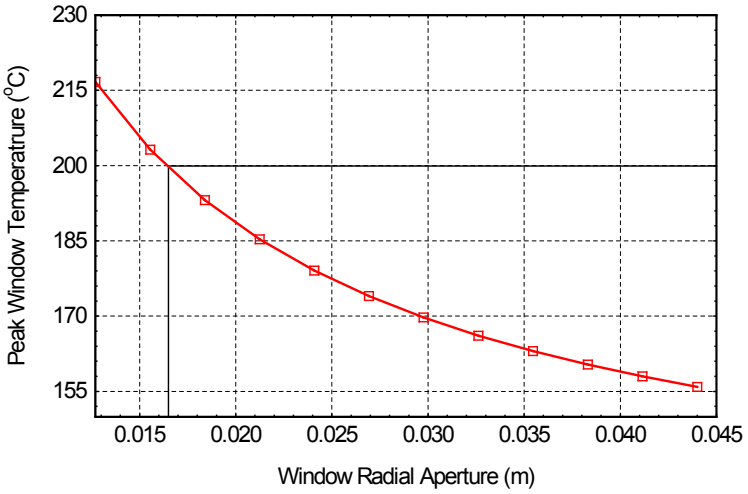

Figure 17. Peak window temperature versus window aperture for Brewster window at 1.5 MW

A major design issue was the choice of window thickness. The cost of the diamond window is roughly proportional to the thickness, and it must be thick enough to withstand the stresses produced by atmospheric pressure and thermal stressed incurred by RF heating and brazing. These stresses were calculated using ANSYS and are summarized in Figure 16.

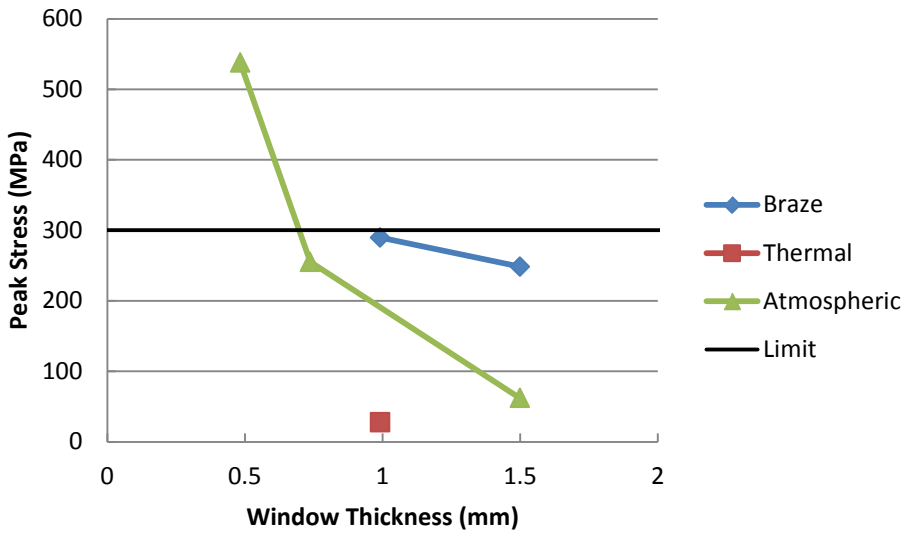

Figure 16. Stresses due to atmospheric pressure and thermal expansion due to RF heating and brazing as a function of window thickness.

The dominant stresses are due to thermal contraction during brazing of the metalized diamond disk into copper seal rings to form the vacuum envelope. There is a 16:1 difference in thermal expansion between copper and diamond. This imposes significant stresses during cooldown during the brazing process. The copper must yield before it imposes destructive stressed on the diamond disk. For a diamond thickness of 1.5 mm, the simulation shown in Figure 18 indicates a 1st principal stress of 200 MPa, compared to the maximum allowable stress of 300 MPa [20]. The predicted maximum von Mises stress in the copper seal ring was 70 MPa with a maximum 1st principal stress of 82 MPa, well below the 250 MPa ultimate strength of copper.

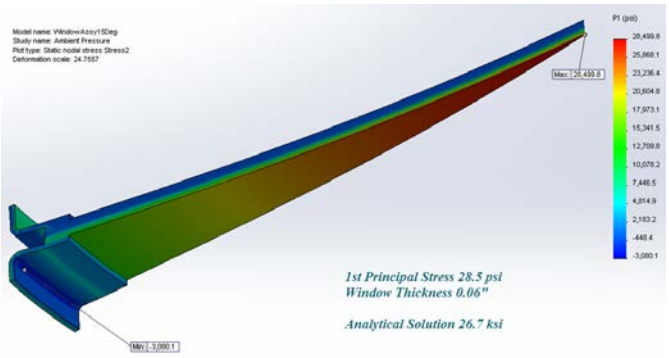

Figure 18. Analysis 1st principal stress in diamond window

The design for the window assembly is shown in Figure 19.

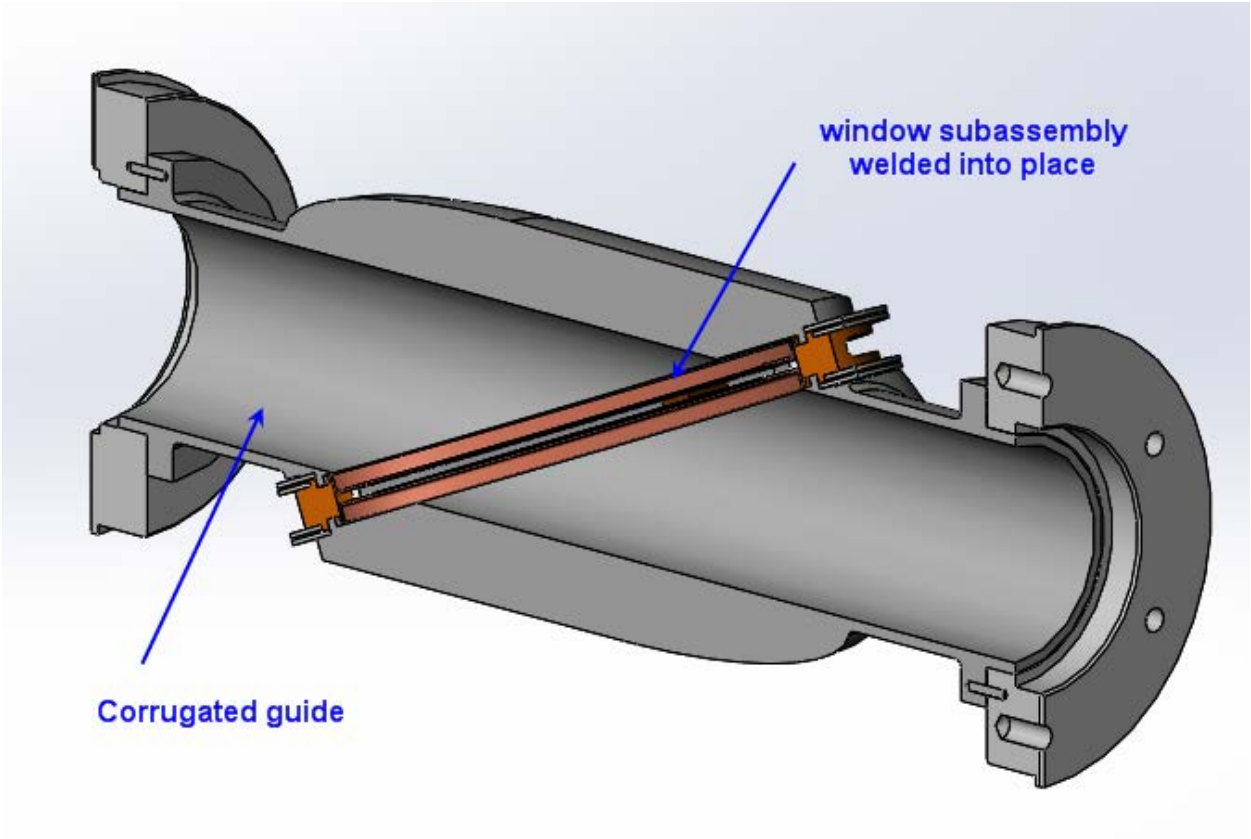

Figure 19. Solid model of the Brewster window. The cooling jacket is not shown.

Figure 20 shows the CVD diamond window assembly following brazing by Communications & Power Industries, LLC in Palo Alto, CA. The window was welded into a vacuum jacket, followed by installation into a cooling jacket. The components of the window assembly are shown in Figure 21. The third component from the left is a sapphire assembly used to test the brazing process prior to risking the diamond disk. The diamond disk assembly is the second component from the right. Figure 22 shows the vacuum envelope prior to installation of the outer cooling jacket, and the completed window assembly is shown in Figure 23.

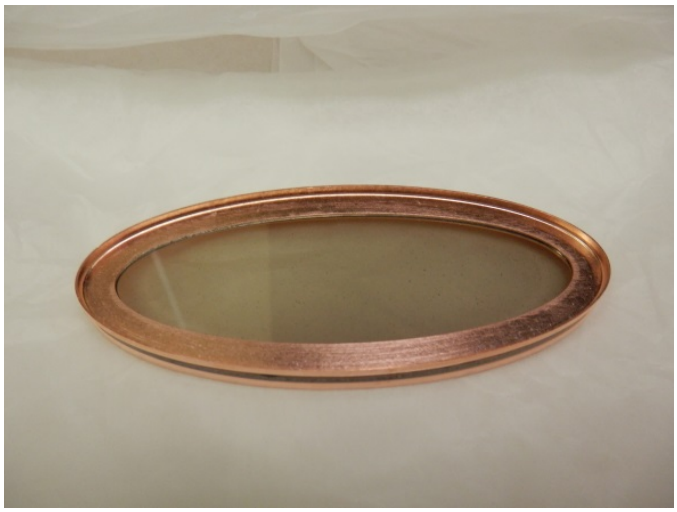

Figure 20. CVD diamond window brazed to copper seal rings

Figure 21. Brewster angle window components

Figure 22. Diamond Brewster angle window vacuum envelope prior to installation of water cooling jacket

Figure 23. Fully assembled CVD diamond Brewster angle window

Testing

Cold Tests

Cold testing of the window was performed at MIT using an Agilent PNA in conjunction with HE_{11} mode launchers [21] provided by General Atomics, Inc. The S11 and S21 measurements for the HE_{11} polarization parallel to the Brewster window normal are shown in Figure 26. The S11 value at 110GHz is about -35dB and the S21 is very small. The S11 and S21 measured for the HE_{11} with polarization perpendicular to the Brewster window normal are shown in Figure 25. The S11 value at 110GHz is about -24dB and the S21 is -8dB.

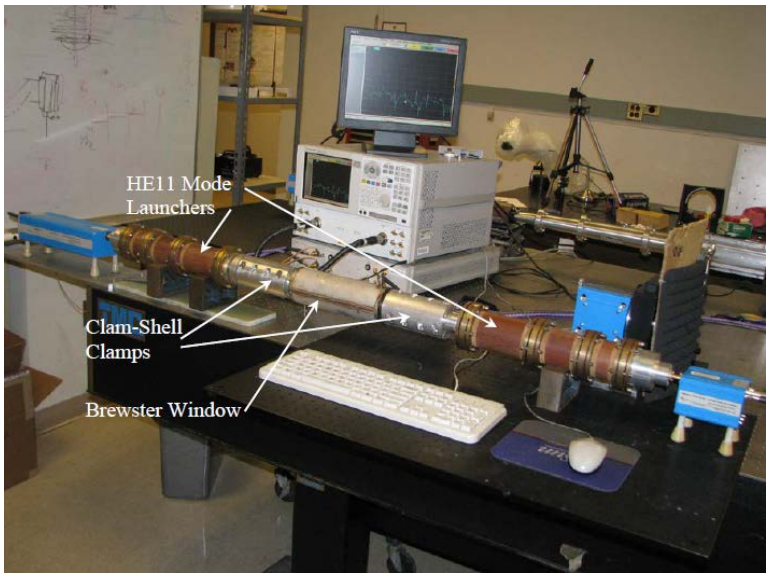

Figure 24. Apparatus for cold testing the Brewster window at MIT.

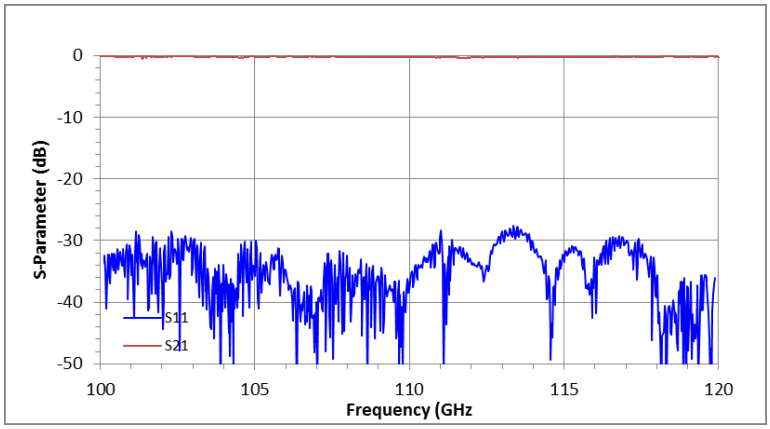

Figure 26. S11

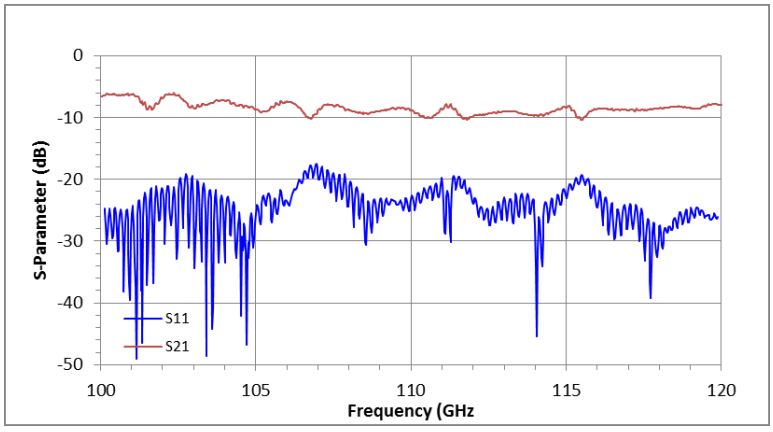

Figure 25. S21

Tests on a 1 MW, 110 GHz Long Pulse Gyrotron

The window was forwarded to General Atomics (GA) in San Diego, CA and installed in an HE_{11} transmission line connected to a 110 GHz, 1 MW gyrotron ("Luke") capable of 5 second pulses. A schematic of the test arrangement is shown in Figure 27, and the gyrotron is shown in Figure 28.

The Brewster window is shown in Figure 29. A quartz window was placed in the waveguide downstream of the Brewster window so vacuum could be pumped down on both sides.

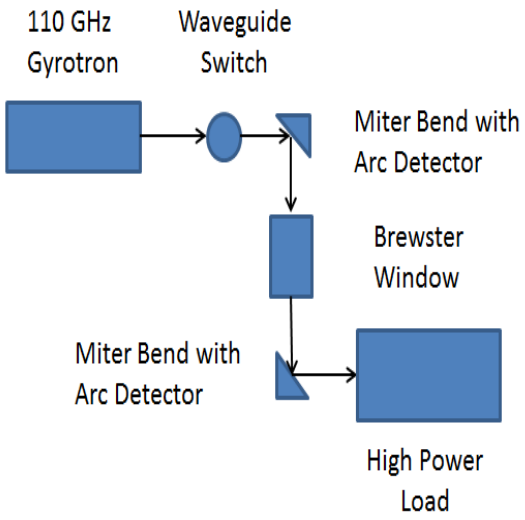

Figure 27. Schematic of the experiment to test the CCR Brewster Window.

Figure 28. "Luke" 1 MW 110 GHz gyrotron used in the tests at GA.

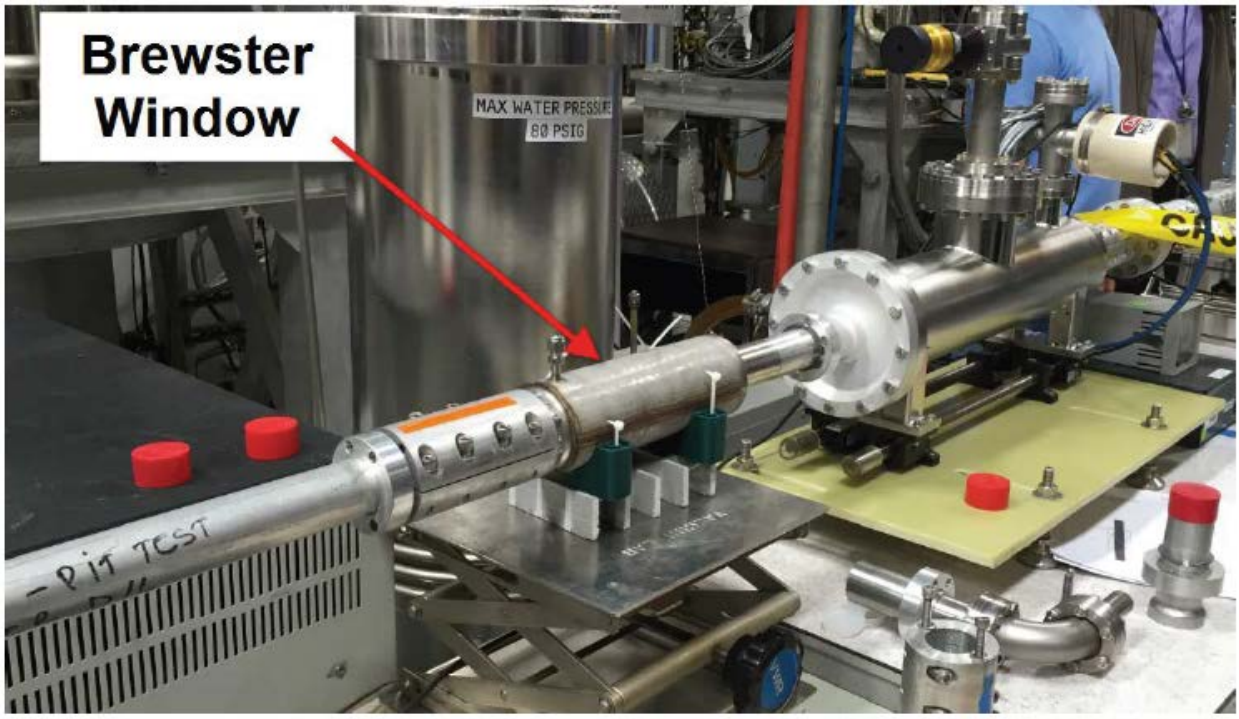

Figure 29. The Brewster Window mounted in HE_{11} guide. The guide at the left brought power from the gyrotron. To the right is a section for pumping the guide. Not shown is the high power load further to the right.

Low power tests confirmed the transmission and polarization.

Testing proceeded carefully to avoid damaging the Brewster angle window. Light flashes from the window were quanititatively monitored using the 4-probe light detector shown in Figure 30. This provided temporal and limited azimuthal information on the location of the light emission.

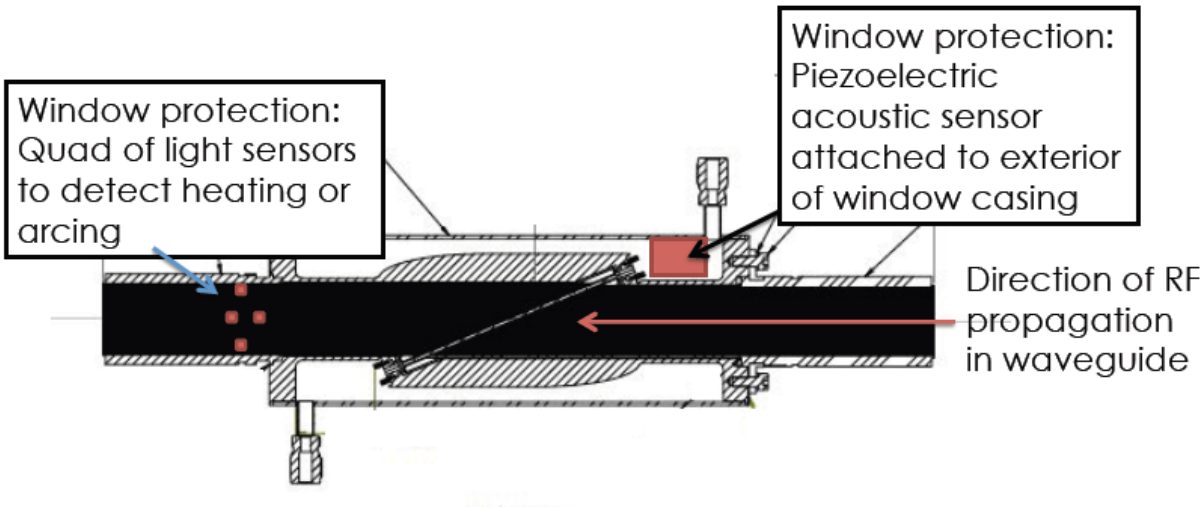

Figure 30. Light detection monitors.

Initial high power, short pulse tests at 400 kW detected no signs of arcing. The power was reduced to 150 kW as the pulse length was progressively increased from 2 msec to 8 msec. There were light signals on the detectors whenever power was increased, but eventually it decreased until it was undetectable. It required 10-20 shots to process the window to eliminate the light signals. GA reported the characteristics of the signals appeared to indicate heating rather than sparking.

As testing progressed, the light sensors detected heating at one azimuthal location. As shown in Figure 31, inspection with a lighted, magnifying borescope detected metal chips from machining the grooves and numerous small flecks on the window surface. GA personnel removed the metal chips as well as surface dust/dirt on the window by dismounting the window and removing the waveguide from one end. The waveguide on the other end is welded in place and could not be removed.

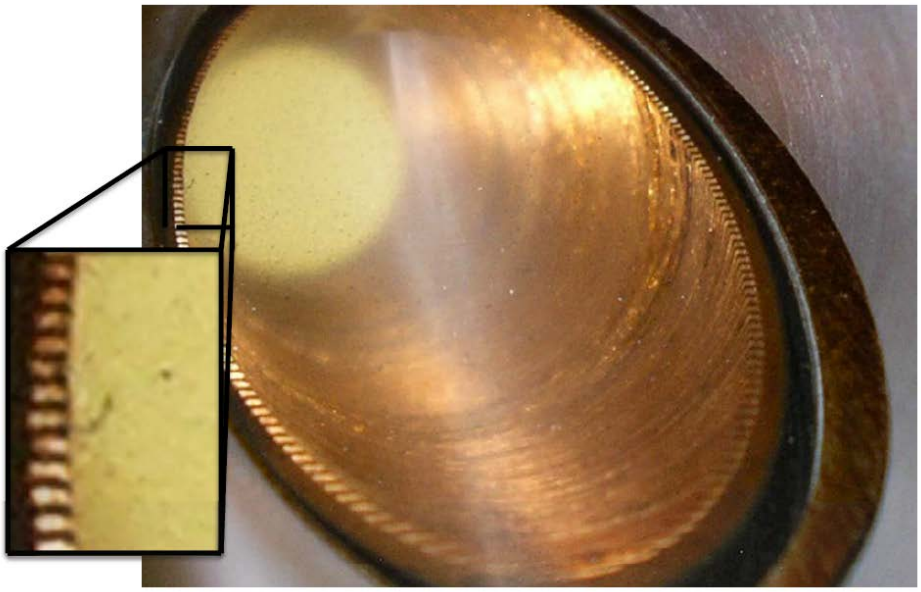

Figure 31. Photo from an inspection microscope showing the structure of the grooves near the

Testing resumed at 100-150 kW with light detected on most every shot. The light signature was more characteristic of heating rather than arcing, so the light detectors were desensitized by approximately a factor of four in two steps. Power transmission was rapidly increased to more than 200 kW with seven msec flattops with no sign of the previous heating, indicating that the source of the heating was burned away.

An exciting observation was that power was detected beyond the Brewster angle window during the rise and fall time of the beam voltage that was not at 110 GHz. This was a clear indication that the window was transmitting power independent of frequency at significant power levels. The measured reflected power was very low or zero.

Calorimetric measurements indicated approximately 500 W of power absorption in the window when transmitting 350 kW in 2 sec pulses. GA added a Delta-T block to the window cooling water circuit to provide a second measurement of the window losses independent of the standard system. The 350 kW output was measured using dummy load calorimetry and was consistent with the gyrotron operating parameters of 34 A, 67.2 kV. The observed loss is significantly larger than expected (100-200 W) based on loss measurements of the diamond disk. It is possible the window became contaminated after the loss measurement, possibly during subsequent welding processes. This is consistent with the observation of localized heating.

There was no indication that the Brewster angle window impacted gyrotron operation, No RF mode hopping was observed, indicating there was insufficient reflection from the window to impact the RF cavity.

GA removed the window in an attempt to determine the source of the oscillatory light signal; however, no obvious source was found. The light monitor section was modified to monitor the window from the gyrotron side. The light signals became more consistent. Close examination of the window detected no noticeable difference from the prior inspection, with flecks still visible on the window. Testing resumed with minimal issues. Equipment was installed to monitor the RF spectrum, looking for parasitic emission or off-mode operation, as the gyrotron operating parameters are somewhat non-standard.

Additional testing was impacted by increased light output due to heating, resulting in arc faults. GA believes these were caused by the specks on the window.

Beam quality was analyzed using a phase retrieval code [24] and measurements using the apparatus shown in Figure 32. The phase retrieval software uses “moments” of the beam to predict the original beam content at the mouth of the waveguide [24]. The gyrotron system did not produce a pure mode, and without the window in place, only 65.2% of the output was in the desired HE_{11} mode. The purity actually increased when the window was installed, resulting in 77.3% of the mode being in the HE_{11} mode. These measurements are shown in Figure 33. The most prevalent other modes were the $LP^{(0)}_{11}$ (2.9% without and 3.6% with) and the LP_{02} (3.7% without and 1.2% with).

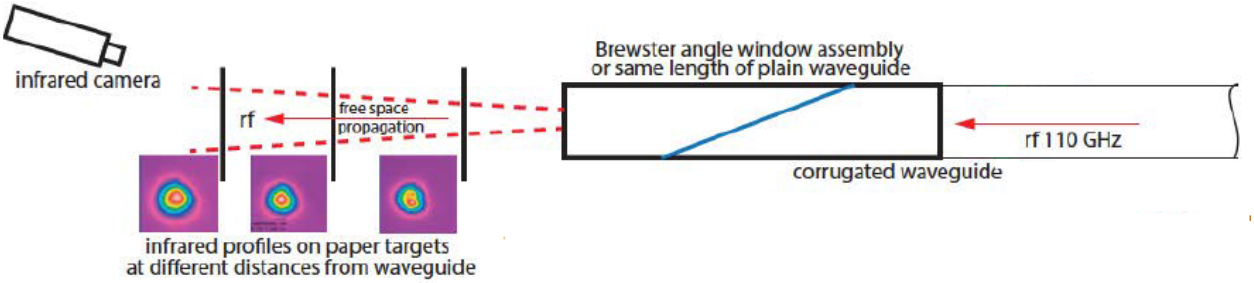

Figure 32. Instrumentation for measurement of the amplitude and phase profiles of the radiation beam.

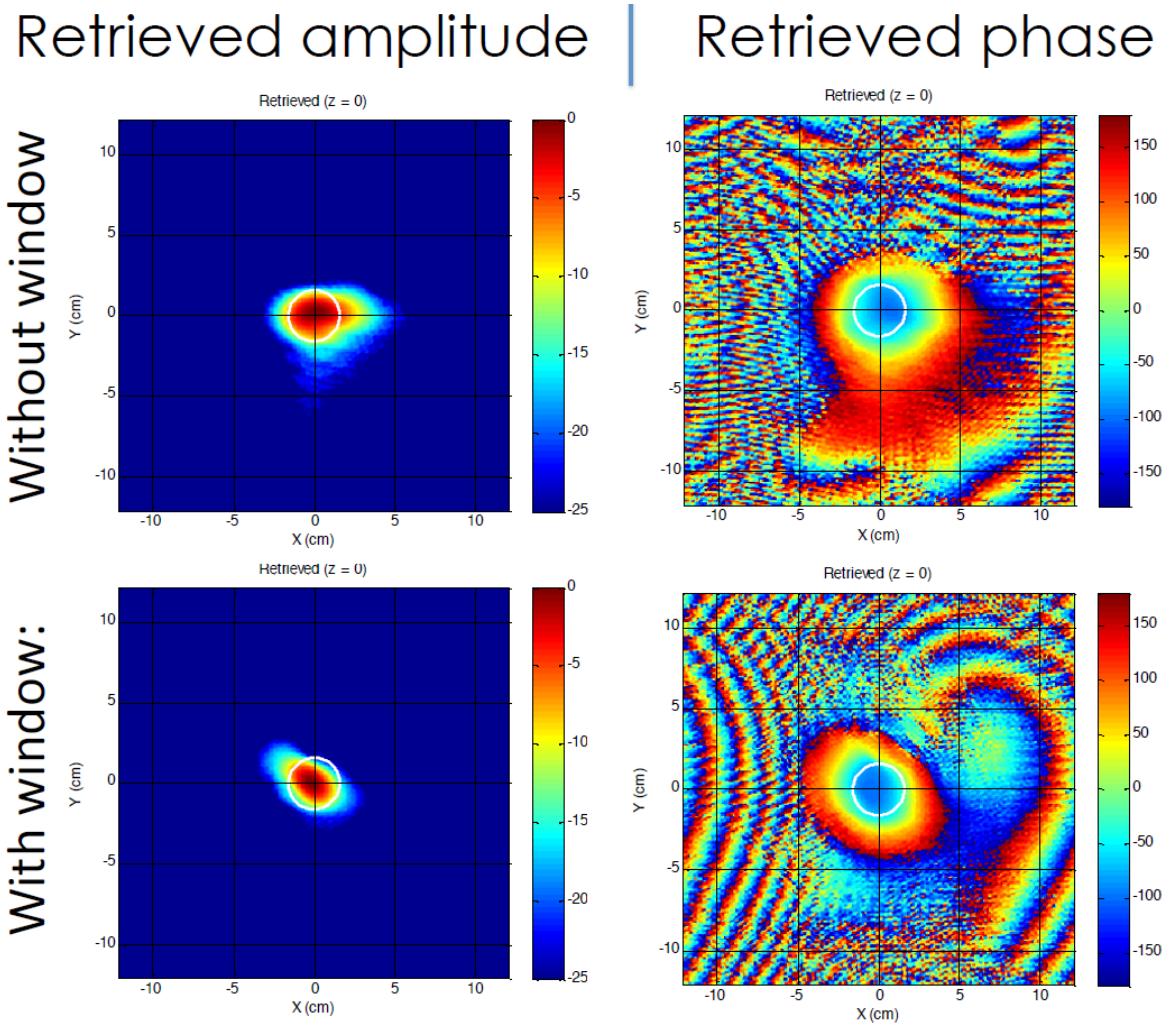

Figure 33. Amplitude and phase measurements of the output radiation without and with the Brewster window.

It is difficult to draw a conclusion from these measurements, other than there was no negative effect from the window on mode purity.

Summary and Conclusion

A direct coupler and Brewster window were designed, fabricated and tested. The advanced coupler converted the gyrotron operating mode of $TE_{22,6}$ into the desired HE_{11} mode with an efficiency of 97.9% and 97.5%, as measured in cold and hot tests, respectively. This is as predicted by theory. This is substantially better than achieved with more complex and costly MOU's. Tests of the effect of the direct coupler on a gyrotron at MIT were inconclusive due to problems with the gyrotron, but there was no evidence that the coupler negatively affected the gyrotron operation. Further tests are planned at MIT.

Cold tests showed that the Brewster window performed as expected. Reflection from the window was below -30 dB over the tested range of 100 GHz to 120 GHz. In tests with a 1 MW gyrotron, radiation patterns showed that the window did not reduce the mode purity.

Losses in the window as measured in the tests with the GA gyrotron were significantly higher than anticipated. It is suspected that this was due to localized impurities in the window as evidenced by light emission from hot spots. These impurities were not evident from loss tangent tests made just after brazing the window. Further examination will be done to try to determine the cause of the losses, but it is not expected that they will be fundamental to the geometry or material. Never-the-less, the localized window heating was large enough that concern with damaging the window resulted in the power to the window being limited to 350 kW, significantly below the design value of 1 MW.

References

1. V. Nichiporenko et al, "Multi-frequency gyrotron for ASCEX Upgrade, 35th International Conference on Infrared, Millimeter, and Terahertz Waves, September 2010.
2. M. Thumm, "MW gyrotron development for fusion plasma applications," Plasma Phys. Control. Fusion 45 (December 2003) A143-A161.
3. H. Zohm, et al., "The physics of neoclassical tearing modes and their stabilization by ECCD in ASDEX Upgrade," Nucl. Fusion 41 (February 2001) 197-202.
4. J.K. Jawla et al, "Design and experimental results for a 527 GHz gyrotron for DNP=NMR spectroscopy," 39th Intern. Conf. Infrared, Millimeter, and THz waves, Tucson, AZ, Sept. 2014.
5. J.R. Sirigiri, et al, "Corrugated transmission line systems for 395/600 MHz and 460 GHz/700 MHz DNP-HNMR spectroscopy," 39th Intern. Conf. Infrared, Millimeter, and THz waves, Tucson, AZ, Sept. 2014.
6. Arnie Kellman, Director Tokamak Systems, General Atomics, private communication, March 2012.
7. A.G. Litvak et al, "New Results of Megawatt Power Gyrotrons Development," Proceedings of IRMMW-THz Conference, 2013.
8. T. Kobayashi et al, "Progress and Status of the Gyrotron Development for the JT-60SA ECH/CD System, 40th International Conference on Infrared, Millimeter, and Terahertz Waves, Hong Kong, August 2015.
9. K. Sakamoto et al, "Progress on High Power Multi-Frequency Gyrotron Development," 37th International Conference on Infrared, Millimeter, and Terahertz Waves (IRMMW-THz), Wollongong, Australia, September 2012.
10. G. Gantenbein et al, "First Operation of a Step-Frequency Tunable 1-MW Gyrotron With a Diamond Brewster Angle Output Window," IEEE Trans. On Electron Devices, Vol. 61, No. 6, pp. 1806 – 1811, June 2014.
11. D. Sobolev and G. Denisov, "Principles of Synthesis of Multimode Waveguide Units", IEEE Trans. Plasma Sci., Vol. 38, No. 10, Oct. 2010.
12. K. Sakamoto et al, "Progress on High Power Long Pulse Gyrotron Development in JAEA," 39th International Conference on Infrared, Millimeter, and Terahertz waves, Tucson, AZ, September 2014.
13. J. Neilson, "Optimal Synthesis of Quasi-Optical Launchers for High Power Gyrotrons", IEEE Trans. Plasma Sci., Vol. 34, No. 3, June 2006.
14. J. Neilson, "Optimization of Quasi-Optical Launchers for Multi-Frequency Gyrotrons", IEEE Trans. Plasma Sci., Vol. 35, No. 6, Dec 2007.
15. U.S. Department of Energy Small Business Innovation Research program DE-FG02-05ER84181, "Advanced Quasioptical Launcher System."
16. William Guss, MIT/PSFC, "Hot Test of CCR Internal Mode Coupler," March 2014.
17. S. Ramo, J.R. Whinnery and T. Van Duzer, Fields and Waves in Communication Electronics, 3rd edition, John Wiley and Sons, Inc, New York, NY, p. 313 (1994).

18. http://www.ga.com/fusionproducts/microwaves/SCWaveguide/index.php
19. Analysis performed by Philipp Borchard at Dymenso, LLC.
20. Kevin Felch, private communication, April 2013.
21. WR8-to-2.35: HE11 Mode Launchers, Part No. 0-9006-0350, Serial No. 12-1, and 12-2.
22. G. Denisov et al, "Multi-frequency gyrotron with BN Brewster Window," 2006 Joint 31st International Conference on Infrared Millimeter Waves and 14th International Conference on Teraherz Electronics, Shanghai, China, September 2006.
23. O. Prinz, G. Gantenbein, M. Thum, "Advanced Quasi-Optical Mode Converter for a Multi-Frequency Gyrotron," IEEE International Vacuum Electronics Conference, 2008.
24. A. LeViness, J. Lohr, J. Anderson, M. Cengher, Y.A. Gorelov, C. Moeller, D. Ponce, A. Torrezan, L. Ives and M. Read, "Testing of a Diamond Brewster Angle Waveguide Window at DIII-D," 58th Annual Meeting of the APS Division of Plasma Physics, Vol 61, Number 18, Abstract JP10.00074, 2016.